Noise performance comparison of 1.5 μm correlated photon pair generation in different fibers

Qiang Zhou,[1, 2] Wei Zhang,[1,*] Jie-rong Cheng,[1] Yi-dong Huang,[1] and Jiang-de Peng[1]

[1]*Tsinghua National Laboratory for Information Science and Technology, Department of Electronic Engineering, Tsinghua University, Beijing 100084, China*

[2]*q-zhou06@mails.tsinghua.edu.cn*

**zwei@mail.tsinghua.edu.cn*

Abstract: In this paper, the noise performances of 1.5 μm correlated photon pair generation based on spontaneous four wave-mixing in three types of fibers, i.e., dispersion shifted fiber, traditional highly nonlinear fiber and highly nonlinear microstructure fiber are investigated experimentally. Result of the comparison shows that highly nonlinear microstructure fiber has the lowest Raman noise photon generation rate among the three types of fibers while correlated photon pair generation rate is the same. Theoretical analysis indicates that the noise performance is determined by the nonlinear index and Raman response of the material in fiber core. The Raman response rises with increasing doping level, while, for the nonlinear index, the impact of doping level is weak. As a result, highly nonlinear microstructure fiber with pure silica core has the best noise performance and great potential in practical sources of correlated photon pairs and heralded single photons.

OCIS codes: (190.4370) Nonlinear optics, fibers; (270.0270) Quantum optics; (270.5585) Quantum information and processing.

References and links

1. J. L. O'Brien, A. Furusawa, and J. Vučković, "Photonic quantum technologies," Nat. Photonics **3**(12), 687–695 (2009).
2. N. Gisin, G. Ribordy, W. Tittel, and H. Zbinden, "Quantum cryptography," Rev. Mod. Phys. **74**(1), 145–195 (2002).
3. S. K. Sharma, D. W. Matson, J. A. Philpotts, and T. L. Roush, """"Raman study of the structure of glasses along the join SiO-GeO," J. Non-Cryst," Sol. **68**, 99 (1984).
4. M. Fiorentino, P. L. Voss, J. E. Sharping, and P. Kumar, "All-fiber photon-pair source for quantum communication," IEEE Photon. Technol. Lett. **14**(7), 983–985 (2002).
5. X. Li, J. Chen, P. Voss, J. E. Sharping, and P. Kumar, "All-fiber photon-pair source for quantum communications: Improved generation of correlated photons," Opt. Express **12**(16), 3737–3744 (2004).
6. H. Takesue, and K. Inoue, "Generation of polarization-entangled photon pairs and violation of Bell's inequality using spontaneous four-wave mixing in a fiber loop," Phys. Rev. A **70**(3), 031802 (2004).
7. H. Takesue, and K. Inoue, "1.5-microm band quantum-correlated photon pair generation in dispersion-shifted fiber: suppression of noise photons by cooling fiber," Opt. Express **13**(20), 7832–7839 (2005).
8. X. Li, P. L. Voss, J. E. Sharping, and P. Kumar, "Optical-fiber source of polarization-entangled photons in the 1550 nm telecom band," Phys. Rev. Lett. **94**(5), 053601 (2005).
9. K. F. Lee, J. Chen, C. Liang, X. Li, P. L. Voss, and P. Kumar, "Generation of high-purity telecom-band entangled photon pairs in dispersion-shifted fiber," Opt. Lett. **31**(12), 1905–1907 (2006).
10. H. Takesue, "1.5 μm band Hong-Ou-Mandel experiment using photon pairs generated in two independent dispersion shifted fibers," Appl. Phys. Lett. **90**(20), 204101 (2007).
11. S. D. Dyer, M. J. Stevens, B. Baek, and S. W. Nam, "High-efficiency, ultra low-noise all-fiber photon-pair source," Opt. Express **16**(13), 9966–9977 (2008).
12. X. Li, L. Yang, L. Cui, Z. Y. Ou, and D. Yu, "Fiber-based source of photon pairs at telecom band with high temporal coherence and brightness for quantum information processing," Opt. Lett. **33**(6), 593–595 (2008).

#129059 - $15.00 USD Received 26 May 2010; revised 16 Jul 2010; accepted 18 Jul 2010; published 28 Jul 2010

13. S. D. Dyer, B. Baek, and S. W. Nam, "High-brightness, low-noise, all-fiber photon pair source," Opt. Express **17**(12), 10290–10297 (2009).
14. L. J. Wang, C. K. Hong, and S. R. Friberg, "Generation of correlated photons via four-wave mixing in optical fibres," J. Opt. B Quantum Semiclassical Opt. **3**(5), 346–352 (2001).
15. J. Sharping, J. Chen, X. Li, P. Kumar, and R. S. Windeler, "Quantum-correlated twin photons from microstructure fiber," Opt. Express **12**(14), 3086–3094 (2004).
16. J. Fulconis, O. Alibart, W. J. Wadsworth, P. St. J. Russell, and J. G. Rarity, "High brightness single mode source of correlated photon pairs using a photonic crystal fiber," Opt. Express **13**(19), 7572–7582 (2005).
17. J. G. Rarity, J. Fulconis, J. Duligall, W. J. Wadsworth, and P. St. J. Russell, "Photonic crystal fiber source of correlated photon pairs," Opt. Express **13**(2), 534–544 (2005).
18. J. Fan, A. Dogariu, and L. J. Wang, "Generation of correlated photon pairs in a microstructure fiber," Opt. Lett. **30**(12), 1530–1532 (2005).
19. J. Fan, A. Migdall, and L. J. Wang, "Efficient generation of correlated photon pairs in a microstructure fiber," Opt. Lett. **30**(24), 3368–3370 (2005).
20. J. Fan, M. D. Eisaman, and A. Migdall, "Quantum state tomography of a fiber-based source of polarization-entangled photon pairs," Opt. Express **15**(26), 18339–18344 (2007).
21. J. Fulconis, O. Alibart, J. L. O'Brien, W. J. Wadsworth, and J. G. Rarity, "Nonclassical interference and entanglement generation using a photonic crystal fiber pair photon source," Phys. Rev. Lett. **99**(12), 120501 (2007).
22. J. Fan, A. Migdall, J. Chen, and E. A. Goldschmidt, "Microstructure-fiber-based source of photonic Entanglement," IEEE J. Sel. Top. Quantum Electron. **15**(6), 1724–1732 (2009).
23. Q. Zhou, W. Zhang, J. Cheng, Y. Huang, and J. Peng, "Polarization-entangled Bell states generation based on birefringence in high nonlinear microstructure fiber at 1.5 microm," Opt. Lett. **34**(18), 2706–2708 (2009).
24. W. Zhang, Q. Zhou, J. R. Cheng, Y. D. Huang, and J. D. Peng, "Impact of fiber birefringence on correlated photon pair generation in highly nonlinear microstructure fibers," Eur. Phys. J. D (to be published).
25. E. Brainis, "Four-photon scattering in birefringent fibers," Phys. Rev. A **79**(2), 023840 (2009).
26. K. Inoue, "Four-wave mixing in an optical fiber in the zero-dispersion wavelength region," J. Lightwave Technol. **10**(11), 1553–1561 (1992).
27. Q. Lin, F. Yaman, and G. P. Agrawal, "Photon-pair generation in optical fibers through four-wave mixing: role of Raman scattering and pump polarization," Phys. Rev. A **75**(2), 023803 (2007).
28. G. P. Agrawal, *Nonlinear Fiber Optics, 4th ed.* (Academic, 2007), Chap. 11.
29. K. Nakajima, and M. Ohashi, "Dopant dependence of effective nonlinear refractive index in GeO_2-andF-doped core single-mode fibers," IEEE Photon. Technol. Lett. **14**(4), 492–494 (2002).
30. S. T. Davey, D. L. Williams, B. J. Ainslie, W. J. M. Rothwell, and B. Wakefield, "Optical gain spectrum of GeO_2-SiO_2 Raman fiber amplifier," IEE Proc., Optoelectron. **136**(6), 301 (1989).
31. S. Fasel, O. Alibart, S. Tanzilli, P. Baldi, A. Beveratos, N. Gisin, and H. Zbinden, "High quality asynchronous heralded single-photon source at telecom wavelength," N. J. Phys. **6**, 163 (2004).

1. Introduction

Correlated photon pairs at 1.5 μm have important applications in quantum communication and quantum information processing [1,2], over large geographic scale, since they are at low loss transmission window of commercial silica fibers. In recent years, correlated photon pair generation through spontaneous four-wave mixing (SFWM) process in optical fibers focuses much attention as a promising way to realizing efficient and compact all-fiber 1.5 μm correlated photon pair sources. However, accompanying with photon pair generation, noise photons would be generated by spontaneous Raman scattering (SpRS), leading to severe deterioration on the performance of 1.5 μm correlated photon-pair generation in fibers. Hence, how to reduce the SpRS noise photons is the key for realizing high quality fiber based 1.5 μm correlated photon pair sources.

According to intensive previous researches on fiber Raman amplification used in optical fiber communications, it is well known that GeO_2 concentration in the fibers changes the Raman response of the fiber, which results from the bond-bending motion of the bridging *O* in the *M*-*O*-*M'* bond (*M* = Si, Ge) [3]. Hence, in fiber based correlated photon pair generation, the property of generated noise photons by SpRS should be different in fibers with different GeO_2-doping levels. Although several types of fibers have been reported to realizing correlated photon pair generation, such as dispersion shifted fiber (DSF) [4–13], traditional single mode fiber [14], microstructure fiber [15–23] and so on, their noise performances have not yet been compared experimentally. In this paper, the noise performances of correlated photon pair generation in DSF, traditional highly nonlinear fiber (HNLF) and highly nonlinear

#129059 - $15.00 USD Received 26 May 2010; revised 16 Jul 2010; accepted 18 Jul 2010; published 28 Jul 2010

microstructure fiber (HNMSF) are investigated experimentally. The comparison results shows that microstructure fiber with pure silica core has a better noise performance, which is preferred for practical all-fiber correlated photon pair source at 1.5 μm.

2. Experiment on correlated photon pair generation in different fibers

The experimental setup for fiber based correlated photon pair generation is shown in Fig. 1. The pulsed pump light is generated from a passive mode locked fiber laser. A filter system based on a fiber Bragg grating, a circulator and a tunable optical band-pass filter (TOBF) (Dicon, TF-1550-0.8-9) is used to extend its pulse width by narrowing its spectrum. Then it is amplified by an erbium dropped fiber amplifier (EDFA). Amplified spontaneous emission of the EDFA is suppressed by another filter system based on two tunable optical band-pass filters, a fiber Bragg grating and a circulator, achieving a side-band rejection of 115 dB at wavelengths where the signal and idler photon detection is performed. The central wavelength, line width and repetition rate of the pulsed pump light are 1552.75 nm, 0.2 nm and 1 MHz, respectively. The duration of the pump pulse is several tens of pico-seconds, estimated by the line width of pump. Before launching the pump pulses into the fiber, a variable optical attenuator (VOA1) and a 50/50 fiber coupler with a power meter (PM) are used to control and monitor the pump level, while, a polarizer (P) followed by a polarization controller (PC) is used to control its polarization state. Correlated photon pairs are generated by SFWM process, accompanied by the noise photons generated by SpRS process, when pump pulses pass through the fiber. The output photons are separated into two parts by a 5/95 fiber coupler. The photons in the 95 percent port are directed into two single photon detectors (SPDs, Id Quantique, id201), through a filtering and splitting system based on a fiber Bragg grating, a 100GHz/40-channels arrayed waveguide grating (AWG, Scion Photonics Inc.), and two tunable optical band-pass filters. Central wavelength and spectral width of the selected signal photons are 1555.15 nm and 0.37 nm, respectively, while 1550.35 nm and 0.37 nm for idler ones, respectively. Total pump isolation is greater than 110 dB at either signal or idler wavelength. The two single photon detectors are operated in gated Geiger mode with a 2.5 ns detection window, and triggered by the pump pulses from the 5 percent port of the coupler detected by a photon detector (PD). The detection efficiencies are 15.01% and 13.85% for SPD1 and SPD2 respectively.

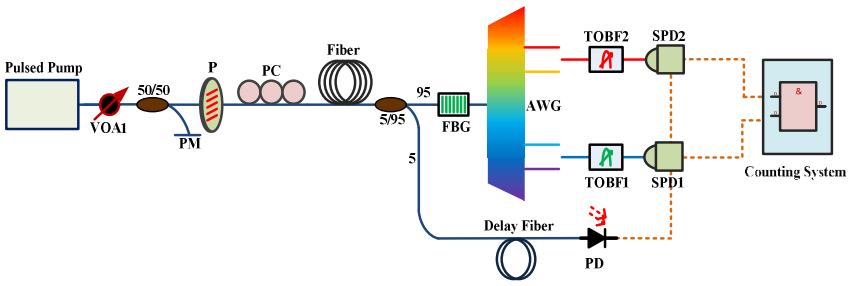

Fig. 1. Experimental setup. VOA, variable optical attenuator; P, polarizer; PM, power meter; PC, polarization controller; FBG, fiber Bragg grating; AWG, arrayed waveguide grating; TOBF, tunable optical band-pass filter; PD, photon detector; SPD, single photon detector.

In the experiment, three types of fibers are used to generate correlated photon pairs, including DSF (G. 653 fiber fabricated by Yangtze Co., Ltd.), traditional HNLF (fabricated by OFS Inc.) and HNMSF (fabricated by Crystal fiber A/S Inc.), respectively. The HNMSF has triangle hole-array in cross-section, the diameters of the silica core and air holes are 1.8 μm and 0.89 μm, respectively. Parameters of the three types of fibers related to correlated photon pair generation are listed in Table 1.

#129059 - $15.00 USD Received 26 May 2010; revised 16 Jul 2010; accepted 18 Jul 2010; published 28 Jul 2010

Table 1. Parameters of three types of fibers used in the experiment

	DSF	Traditional HNLF	HNMSF
Optical nonlinear coefficient	3 /W/km	11.1 /W/km	66.7 /W/km
Phase birefringence	–	–	3.5×10^{-5}
Dispersion at the pump wavelength	0.05 ps/km/nm	0.076 ps/km/nm	8.65 ps/km/nm
Zero dispersion wavelength	1549 nm	1548 nm	1564.1 nm
Length	1000 m	500 m	25 m

Four photon count rates are measured in the experiment. The single-side photon count rates of the signal and idler photons are denoted by N_s and N_i, respectively. N_{co} denotes the coincident count rate, representing the result that both single photon detectors record photons simultaneously and the detected photons are generated by the same pump pulse. N_{ac} denotes the accidental coincident count rate, representing the result that both single photon detectors record photons simultaneously, but they are generated by different pump pulses. N_{co} and N_{ac} can be measured by a counting system with a coincident logic circuit. All the experimental data is obtained and averaged under a count time of 30 seconds.

Firstly, correlated photon pair generation is demonstrated under different pump power level using DSF. Figure 2 (a) and (b) show the measured single-side photon count rates at the signal and idler side. A second-order polynomial, $N_s, N_i = s_1 N_p + s_2 N_p^{\,2}$, is used to fit the experimental data, in which s_1 and s_2 are the linear and quadratic fitting coefficients, N_p is the pump photon number per pulse, the quadratic term (dashed line) represents the contribution of the photon generated through SFWM process, while the linear term (solid line) represents the contribution of the noise photon generated through SpRS process. Experimental results show s_1 = 5.315 and s_2 = 6.485 for the signal photon, while s_1 = 3.82 and s_2 = 4.13 for the idler photon, showing that photons detected in either side have the contribution of SFWM process. Figure 2 (c) gives the coincident and accidental coincident count rates with increasing signal side photon count rates. It can be seen that the coincident count rates (square dots) are obviously higher than the accidental coincident rates (circular dots), demonstrating the quantum correlation of generated signal and idler photons. The quantum correlated property of the generated photons in the experimental setup is also demonstrated by observing the ratios between N_{co} and N_{ac} under a fixed idler side wavelength (1550.35 nm) and different signal side wavelengths, which can be realized easily by selecting different signal side channels of the arrayed waveguide grating. Figure 2 (d) shows the experimental results. A ratio of 4.24 is achieved under a signal side wavelength of 1555.15 nm, while, the ratios are about 1 under other signal side wavelengths, indicating the correlation in wavelength of the generated photon pairs. Similar experimental results also can be obtained using traditional HNLF and HNMSF, showing that correlated photon pairs can be generated and detected successfully in the experimental setup using all the three types of fibers.

The relatively low ratio between N_{co} and N_{ac} is due to the non-correlated noise photons generated by SpRS process. In order to investigate the impacts of SpRS noise photons on the correlated photon pair in different fibers, real generation rates of correlated photon pair, stokes and anti-stokes SpRS photons should be obtained. In the experiment, the four photon count rates measured in the experiment can be expressed as

$$\begin{aligned} N_s &= \eta_s(R + R_s) + d_s, \\ N_i &= \eta_i(R + R_i) + d_i, \\ N_{co} &= \eta_s\eta_i(R + RR_s + RR_i + R_sR_i) + \eta_s(R + R_s)d_i + \eta_i(R + R_i)d_s, \\ N_{ac} &= \eta_s\eta_i(R^2 + RR_s + RR_i + R_sR_i) + \eta_s(R + R_s)d_i + \eta_i(R + R_i)d_s. \end{aligned} \tag{1}$$

#129059 - $15.00 USD Received 26 May 2010; revised 16 Jul 2010; accepted 18 Jul 2010; published 28 Jul 2010

Here, R is the generation rate of the correlated photon pairs by SFWM process. R_s and R_i is the generation rates of stokes and anti-stokes SpRS photons at signal and idler wavelengths, respectively. d_s and d_i are the dark count rates of SPD1 and SPD2, respectively. The measured photon count rates are also impacted by the collection efficiencies of signal and idler photons, which are determined by losses of the filtering and splitting system and detection efficiencies of the two SPDs. The collection efficiencies are denoted by η_s and η_i for the signal and idler photons, respectively. Since the dark counting rates and the collection efficiencies can be measured during the experimental setup preparation, R, R_s and R_i can be obtained from the experimental data of the four photon count rates according to Eq. (1).

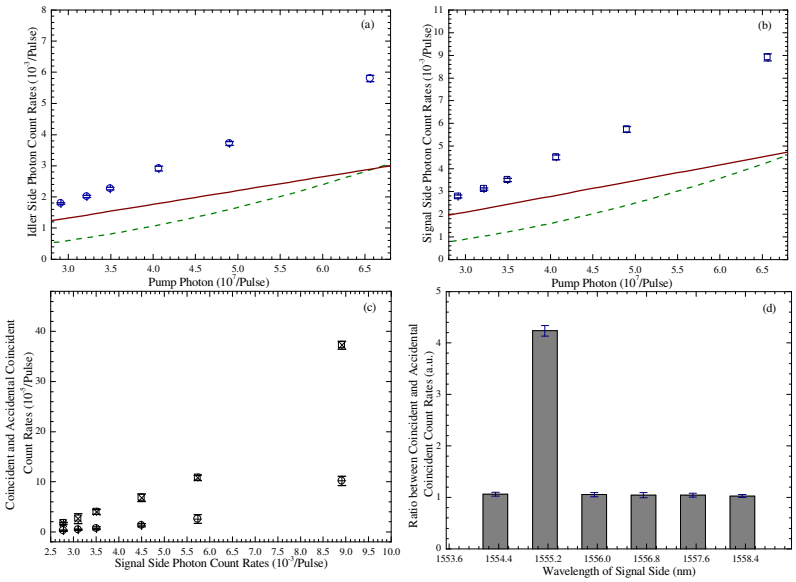

Fig. 2. Experimental results of correlated photon pair generation and quantum correlation property of the generated photons in DSF. Figure 2 (a), (b) the single side count rates of idler and signal photon, respectively; Fig. 2 (c) the coincident (square dots) and accidental coincident (circular dots) count rates under increasing signal side count rate; Fig. 2 (d) the ratio between coincident and accidental coincident counts under six different signal side wavelengths.

In the experiment, the four photon count rates in DSF, traditional HNLF and HNMSF under increasing pump level are measured, respectively. Then R, R_s and R_i in different fibers are calculated according to the experimental data and Eq. (1). It is worth noting that since the splicing losses between single mode fiber and the three types of fiber used in the experiment are different, η_s and η_i are collimated before the experiment for each type of fiber, which is given in Table 2. On the other hand, our previous work shows that correlated photon pair generation in HNMSF is influenced by its birefringence [23,24]. Hence, in the experiment the polarization direction of pump light is set to one of the polarization axes of the HNMSF by adjusting PC1 to avoid the influence of fiber birefringence.

Table 2. Collection efficiencies for signal and idler photons for three types of fibers in the experiment

	Signal photons (η_s) %	Idler photons (η_i) %
DSF	5.84	6.63
Traditional HNLF	4.53	4.70
HNMSF	3.29	3.48

#129059 - $15.00 USD Received 26 May 2010; revised 16 Jul 2010; accepted 18 Jul 2010; published 28 Jul 2010

Figure 3 is the calculated R, R_s and R_i under increasing pump level in DSF, traditional HNLF and HNMSF, shown in Fig. 3 (a), (b) and (c), respectively. The square, circular, and triangular dots are the experimental results of R, R_s and R_i, respectively, while, the solid, dash-dotted and dashed lines are the fitting curve of them, respectively. As shown in Fig. 3, R increases with pump level quadratically, while, R_s and R_i linearly increase with pump level.

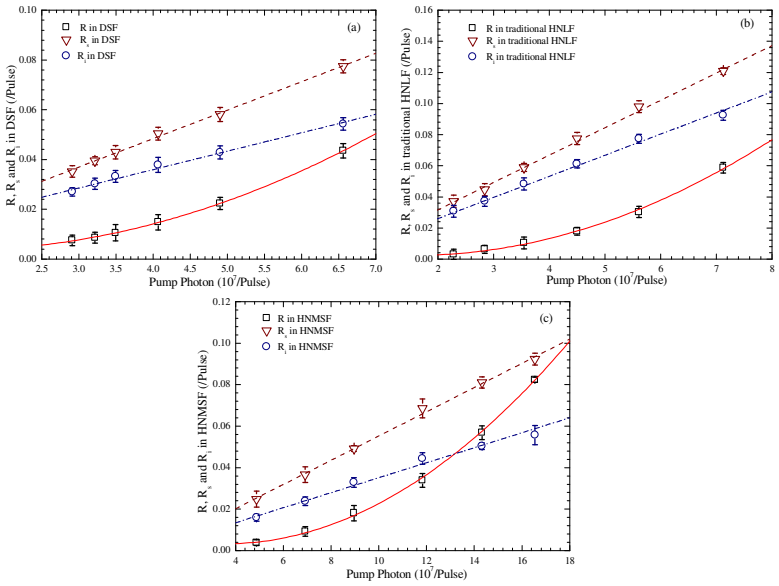

Fig. 3. R, R_s and R_i under increasing pump level in DSF (Fig. 3 (a)), traditional HNLF (Fig. 3 (b)) and HNMSF (Fig. 3 (c)). The square, circular and triangular dots are experimental results of R, R_s and R_i respectively. The solid line, dashed-dot line and dashed line are the fitting curves of them.

It can be seen that SpRS noise photons have large contributions to the generated photons in all the three types of fibers in room temperature under a correlated photon pair generation rate of 0.01~0.1/pulse, which ensures sufficient low multi-photon pair possibility in one pulse. Hence, it can be expected that SpRS noise photons will largely worsen the performance of applications of fiber based correlated photon pair sources. For example, if they are used as heralded single photon sources (HSPSs), in which the idler photons are detected by single photon detector, providing electrical triggers for the arrival of signal photons. The preparation efficiency of fiber based HSPSs is determined by the noise performance of correlated photon pair generation and the signal side loss, including component losses in filtering and splitting system and slicing loss between fibers, which can be reduced by proper design of filtering and splitting system, component selection and fiber slicing technique. Hence, the noise performance determines the theoretical up-limit of HSPS preparation efficiency, which is $R/(R+R_i)=1/(1+R_i/R)$, considering that R and R_i are sufficient low and SpRS noise photons do not have quantum correlation characteristics.

To compare the noise performance of correlated photon pair generation in different types of fibers, the ratios between R and R_i in the three types of fibers under increasing R are plotted in Fig. 4. The circular, square and triangular dots are the ratios in HNMSF, DSF and traditional HNLF respectively while the solid, dashed and dashed-dot lines are fitting curves using $y=A\sqrt{R}$, A is the fitting parameter, which will be discussed in the following section. It can be seen that in all the fibers the ratio between R and R_i increases in square root function.

#129059 - $15.00 USD Received 26 May 2010; revised 16 Jul 2010; accepted 18 Jul 2010; published 28 Jul 2010

The HNMSF shows the best noise performance, while the traditional HNLF shows the worst one. Under the same R, R_i in HNMSF is about half of the one in traditional HNLF.

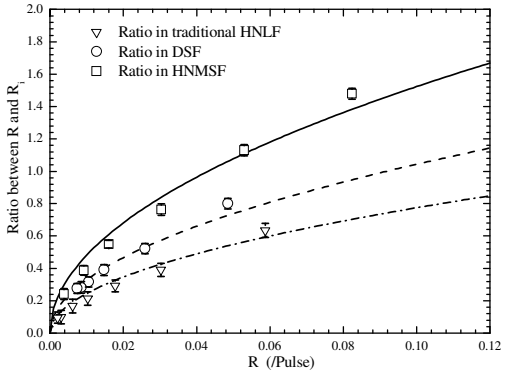

Fig. 4. The ratio between R and R_i. The circular, square and triangular dots are the ratio in DSF, HNMSF and traditional HNLF, respectively, while the solid, dashed and dashed-dot lines are the fitting curves of them.

3. Discussion

In the experiment, the generation rates of photons, R, R_s and R_i can be expressed as $\Delta\nu\tau\xi_c(\Omega)\big|_{\Omega=0.3THz}$, $\Delta\nu\tau\xi_s(\Omega)\big|_{\Omega=0.3THz}$ and $\Delta\nu\tau\xi_i(\Omega)\big|_{\Omega=0.3THz}$, respectively. Where, $\Delta\nu$ and τ are the bandwidth of filtering and splitting system and the detection window width of SPDs, which are about 50 GHz and several tens of pico-seconds in both signal and idler sides in the experiment, respectively. Ω is the frequency detuning between the pump light and the generated photon, Ω = 0.3 THz in the noise comparison experiment. $\xi_c(\Omega)$, $\xi_s(\Omega)$ and $\xi_i(\Omega)$ are the photon flux spectral densities of the correlated photon pairs, anti-stokes SpRS photon and stokes SpRS photon, respectively. According to the quantum theory of photons generation in fibers [25–27], $\xi_c(\Omega)$, $\xi_s(\Omega)$ and $\xi_i(\Omega)$ under a co-polarized single-pump configuration can be obtained by

$$\begin{aligned}
\xi_c(\Omega) &= \left|\gamma P_0 L\right|^2 \sin c^2\left[\left(\sum_{m=1}^{+\infty}\left(\frac{2\beta_{2m}}{(2m)!}\Omega^{2m}\right)+2\gamma P_0\right)\frac{L}{2}\right],\\
\xi_i(\Omega) &= P_0 L g_R(\Omega)\left[\exp\left(\hbar|\Omega|/k_B T\right)-1\right]^{-1},\\
\xi_s(\Omega) &= P_0 L g_R(\Omega)\left[\left(\exp\left(\hbar|\Omega|/k_B T\right)-1\right)^{-1}+1\right].
\end{aligned} \tag{2}$$

Here, P_0 is the power of pump light. L is the length of fiber. $\beta_{2m} = \left(d^{2m}\beta/d\omega^{2m}\right)_{\omega=\omega_p}$ are the even-order fiber dispersions at the pump frequency ω_p. T is the temperature of the fiber. γ and g_R are fiber nonlinear coefficient and co-polarized Raman gain coefficient, respectively.

From Eq. (2), it can be seen that the spectral profile of $\xi_c(\Omega)$ is determined by the *Sinc* function. In experiments of correlated photon pair generation, the pump level is quite low, leading to a flat region near the pump frequency (where Ω is small). The value of $\xi_c(\Omega)$ in this region is close to the maximum of it, which is determined by $\left|\gamma P_0 L\right|^2$ whatever the type of

#129059 - $15.00 USD Received 26 May 2010; revised 16 Jul 2010; accepted 18 Jul 2010; published 28 Jul 2010

fiber. Figure 5 shows the generation rates of photon pairs with different frequency detuning in the three types of fibers, which are achieved by measuring N_s, N_i, N_{co} and N_{ac} at different correlated ports of the arrayed waveguide grating and calculated the photon pair generation rate R through Eq. (1). Figure 5 (a) is the result of DSF under a pump level of 7.2×10^7 photons per pulse. The results of traditional HNLF and HNMSF are shown in Fig. 5 (b) and (c) under pump levels of 7.16×10^7 and 14.5×10^7 photons per pulse, respectively. It can be seen that the measured R with different frequency detuning is almost unchanged in all the three types of fibers, indicating that the measured photon pairs are all in the flat region near the pump frequency.

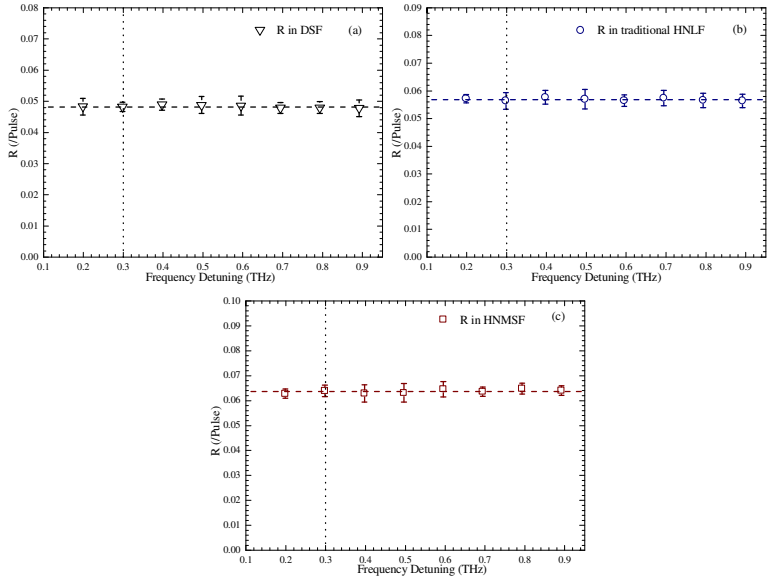

Fig. 5. Correlated photon pair generation rates under different frequency detuning in DSF (Fig. 5 (a)), traditional HNLF (Fig. 5 (b)) and HNMSF (Fig. 5 (c)) with the pump level of 7.2×10^7, 7.16×10^7 and 14.5×10^7 photon per pulse, respectively.

The dotted lines in the figures indicate the frequency detuning of the detected signal and idler photons in the experiment of noise performance comparison, which is about 0.3 THz and in the flat region under all the pump levels in all the three types of fibers. Hence, the impact of phase-matching can be neglected in the theoretical analysis of the experimental results shown in Fig. 4. Under this simplification, the photon pair generation rate R increases quadratically with increasing pumping level in all the three types of fibers, which is demonstrated by the experimental result in Fig. 3. A simplified expression of the ratio between R and R_i, which is denoted by $\kappa(\Omega)$, can be deduced as

$$\kappa(\Omega)\big|_{\Omega=0.3THz}=\frac{R}{R_i}\Big|_{\Omega=0.3THz}=\frac{\gamma\sqrt{R}}{g_R(\Omega)\left[\exp\left(\hbar|\Omega|/k_BT\right)-1\right]^{-1}\sqrt{\Delta\nu\tau}}\Big|_{\Omega=0.3THz}. \quad (3)$$

Equation (3) is the origin of the fitting function $y=A\sqrt{R}$ in Fig. 4. The fitting parameter A should be $\dfrac{\gamma}{g_R(\Omega)\left[\exp\left(\hbar|\Omega|/k_BT\right)-1\right]^{-1}\sqrt{\Delta\nu\tau}}\Big|_{\Omega=0.3THz}$, which is a constant determined by

#129059 - $15.00 USD Received 26 May 2010; revised 16 Jul 2010; accepted 18 Jul 2010; published 28 Jul 2010

the fiber properties and fiber temperature. The impact of fiber temperature has been investigated comprehensively in previous works [7,12]. Our work is focused on the impact of fiber properties.

Equation (3) shows that fiber with high nonlinear coefficient and low Raman gain coefficient is preferred for fiber based correlated photon pair generation with low SpRS noise photons. In fibers, $\gamma \propto n_2 / A_{eff}$, where, n_2 is the nonlinear refractive index of the material in fiber core and A_{eff} is the effective area of the fiber. While, $g_R \propto g / A_{eff}$, where g is the Raman response of it. It can be seen that under the same R and fiber temperature, $\kappa(\Omega)$ is determined by the nonlinear optical characteristics of the material in fiber core. In order to improve γ and g_R in traditional fibers, the usual way is reducing the GeO_2-doping core size and enhancing the GeO_2-doping level in the fiber core. It can reduce A_{eff} of the fiber, which will enhance either γ or g_R. On the other hand, previous works show that g of the fiber core material is highly dependent on the GeO_2-doping level. Comparing with normal single mode fiber (SMF), g can be improved by several times in high GeO_2-doping fiber. However, n_2 shows a weak dependence on the GeO_2-doping level. The measured value of n_2 varies in a range from 2.2×10^{-20} to 3.9×10^{-20} m^2/W, depending on the measuring technique and fiber type [28–30]. As a result, the Raman gain coefficient g_R increases faster than nonlinear coefficient γ with increasing GeO_2-doping level. Hence, comparing with DSF, noise performance of the correlated photon pair generation in traditional HNLF is worse due to a higher doping level. On the other hand, HNMSF has pure silica core and its high γ is achieved by reducing the core size and extending the air hole fraction. Hence, correlated photon pair generation in HNMSF has the best noise performance among the three types of fibers, which agrees well with the experimental results shown in Fig. 4.

To show the impact of fiber property on the performance of applications on fiber based correlated photon pair sources. The theoretical up-limit of the HSPS preparation efficiency is calculated by $R/(R+R_i) = 1/(1+1/\kappa(\Omega))\big|_{\Omega=0.3THz}$, using the fitting curves in Fig. 4 and Eq. (3). Figure 6 shows the results in the room temperature (300 K) and typical temperature achieved by Peltier cooling technique (173 K). The gray solid, dashed and dashed-dot lines correspond to the result of HNMSF, DSF and traditional HNLF in 300 K, respectively, while, the black solid, dashed and dashed-dot lines correspond to the result of them in 173 K, respectively. The dotted line in the figure indicates a typical correlated photon pair generation rate of 0.1/pulse. Under different temperature, R is almost unchanged and R_i should be modified under different temperature through Eq. (2). It can be seen that under all the conditions (whatever the fiber type and the fiber temperature) the preparation efficiency increases with R, thanks to R increases faster than R_i with the pump level as shown in the experimental result in Fig. 3. Under a certain fiber temperature and R, HNMSF has the highest preparation efficiency due to its best noise performance among the three types of fibers. It can be seen that, for a typical R of 0.1/pulse (possibility of multi-photon is about 0.45%), the theoretical up-limit of preparation efficiency of the HNMSF based HSPS is 60.37% under room temperature, which is even higher than that based on traditional HNLF under 173 K. If the HNMSF is refrigerated to 173 K, the theoretical up-limit of preparation efficiency would be 72.85%, which is close to the highest level of HSPS based on correlated photon pair generation by spontaneous parametric down conversion (SPDC) in nonlinear crystal [31]. Hence, HNMSF has great potential in practical sources of correlated photon pairs and heralded single photons, employing proper design of splitting and filtering system, improved fiber splicing technique and Peltier cooling technique.

#129059 - $15.00 USD Received 26 May 2010; revised 16 Jul 2010; accepted 18 Jul 2010; published 28 Jul 2010

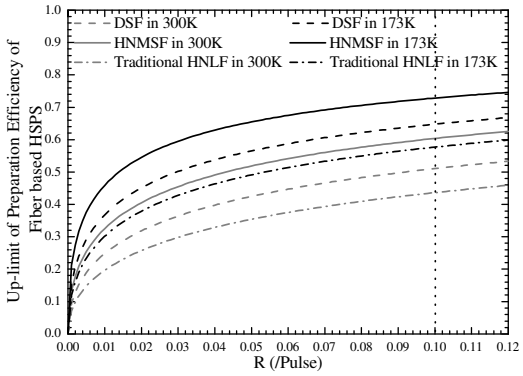

Fig. 6. The up-limit of preparation efficiency of fiber based HSPS under 173K. The solid, dashed and dashed-dot lines correspond to the HNMSF, DSF and traditional HNLF, respectively.

4. Conclusion

In this paper, the noise performances of 1.5 μm correlated photon pair generations in DSF, HNLF and HNMSF, are investigated experimentally. Result of comparison indicates that HNMSF has the lowest Raman noise photon generation rate among the three types of fibers while correlated photon pair generation rate is the same. Theoretical analysis shows that the noise performance is determined by the nonlinear index and Raman response of the material in the core of fiber. The Raman response rises with increasing doping level, while, for the nonlinear index, the impact of doping level is weak. As a result, HNMSF with pure silica core has the best noise performance and has great potential in practical sources of correlated photon pairs and heralded single photons.

Acknowledgements

This work is supported in part by National Natural Science Foundation of China (NNSFC) under Grant No. 60777032, 973 Programs of China under Contract No. 2010CB327600, Science Foundation of Beijing under Grant No. 4102028, and Basic Research Foundation of Tsinghua National Laboratory for Information Science and Technology (TNList).

#129059 - $15.00 USD Received 26 May 2010; revised 16 Jul 2010; accepted 18 Jul 2010; published 28 Jul 2010